Flight Control System Design for an In-Flight Simulator

F. Henschel*
DFVLR, Braunschweig, Federal Republic of Germany
and
S. Chetty*
NAL, Bangalore, India

This paper describes the theoretical development and nonlinear digital simulation results of the model-following flight control system for a new in-flight simulator. A detailed description of the manner in which the feedforward and feedback gains are obtained using an interactive computer-aided-design technique is given. Additional filters in the forward loop enable the feedforward gains to be made independent of the model aircraft parameters even when the actuator dynamics are modeled explicitly. The feedback gains are obtained by using a vector optimization technique. Several time- and frequency-domain measures are used to obtain the required performance. Modified robustness measures based on singular-value decomposition are used to constrain the feedback gains. The sensitivity of the model-following system to changes in flight condition is minimized using a multimodel formulation. Nonlinear simulation results are presented to show the quality of the model-following system and to substantiate the theory and design procedure.

Nomenclature

A = system dynamics matrix
B = control input matrix
c_i = elements in the weighting vector
D = matrix defining the integral states
e = model-following error vector
$G(s)$ = transfer-function matrix
g_i = row vector in the transfer-function matrix
J_i = elements in the performance index vector
K_1 = proportional feedback gain matrix
K_2 = integral feedback gain matrix
L = maximum number of performance index vector elements
n = dimension of the state vector
p = dimension of the control vector
q = pitch rate
R = actuator input matrix
s = Laplace variable ($j\omega$)
t = time
T_s = sampling time
$\boldsymbol{u}$ = control input vector
V = actuator dynamic matrix
$\boldsymbol{w}$ = error integral vector
$\boldsymbol{x}$ = state vector
Y = actuator output vector
$\bar{y}$ = vector defined in Eq. (4c)
α = angle of attack
α_i = real part of the input
β_i = imaginary part of the input vector
δ_e = elevator position
δ_f = flap position
δ_{th} = throttle position
$\boldsymbol{\eta}$ = error vector in Eq. (4c)
θ = pitch angle
$\bar{\sigma},\underline{\sigma}$ = maximum, minimum singular values
σ_{di},σ_{si} = individual singular values
ω = angular frequency, rad/s

Subscripts
D = disturbance
F = feedforward
$i,2$ = indices
m = model
R = feedback

Superscripts
T = transpose of matrices and vectors
$+$ = pseudoinverse of a matrix
-1 = inverse of a square matrix

Received June 19, 1987; presented as Paper 87-2451 at the AIAA 1987 Guidance, Navigation, and Control Conference, Monterey, CA, Aug. 17-19, 1987; revision received March 28, 1988.

*Research Assistant.

Introduction

THE theoretical development and nonlinear simulation results of the model-following system for the new in-flight simulator Advanced Technologies Testing Aircraft System (ATTAS) are described. The experimental aircraft is a modified version of the VFW-614 transport aircraft (Fig. 1) and is equipped with a wide range of sophisticated sensors, instrumentation, and electronics.[1] These subsystems communicate with the servoactuators through a network of high-performance computers that can be configured to simulate a broad spectrum of the state-of-the-art and a futuristic aircraft system in actual flight. The rear part of the landing flaps has been divided into six fast-moving flaps (three on each wing) with a flap actuation rate of 75 deg/s (under aerodynamic loads) and ± 35-deg flap deflection for high-frequency direct lift modulation. In addition the engines, rudder, elevator, and ailerons (both symmetric and differential modes) are driven by self-monitored electrohydraulic actuators, thus giving the vehicle a five degree-of-freedom in-flight simulation capability.

In comparison to previous design techniques reported in the literature, this method allows the designer to compensate the phase lag introduced by the actuators of the host aircraft. In addition, the other performance requirements, including sensitivity minimization to changes in flight condition, can be directly addressed by formulating each of these requirements as individual elements of the performance index vector (PIV).

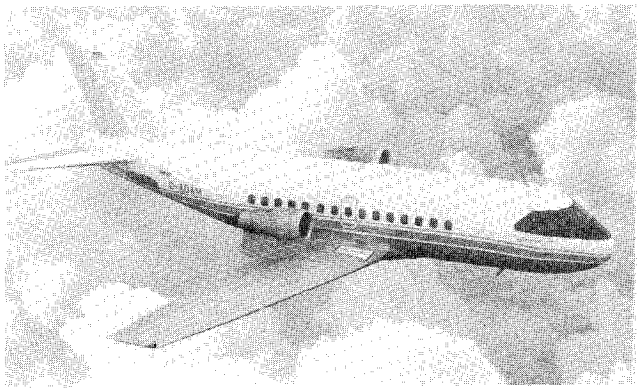

Fig. 1 ATTAS

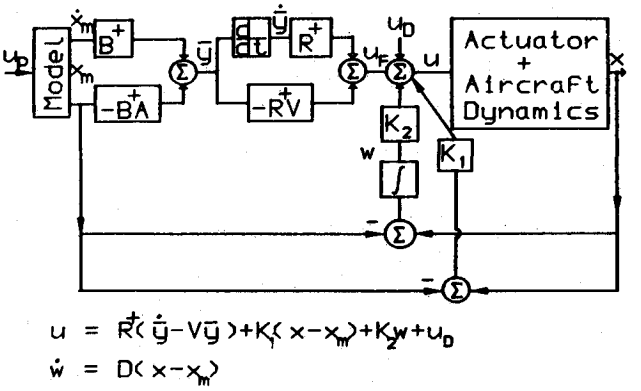

Fig. 2 Model-following control system for in-flight simulation.

Nonlinear digital simulation results in the form of overlays of the model and ATTAS time histories are presented to show the quality of model following and to substantiate the theory and design procedure.

Design

In-flight simulators are flying platforms designed to provide realistic vision and motion cues. This simulation technique allows the investigation of complex interactions between the pilot and the model in demanding flight situations, e.g., during a landing or when certain subsytems fail.

Therefore, the main objective of the model-following control system is to make the host aircraft duplicate the flight path, attitudes, transients, and control characteristics of the model in flight with sufficient fidelity. Theoretically, exact model following can be achieved by using either a feedforward or feedback controller; however, past experience[2–6] has shown the need to use a combination of feedforward plus feedback control to ensure good model-following quality in flight. Control deflections required for model following are determined primarily by the feedforward gains between the model and the host aircraft. The feedback gains are selected to ensure rapid and smoothly decaying error dynamics in the presence of external disturbances, sensor noise, system nonlinearities, etc, and to maintain the quality of model following, which would otherwise rapidly deteriorate as flight conditions change.

Feedforward Control

Let the plant and the model be described in standard state-space form as

$$\dot{x} = Ax + Bu \tag{1}$$

where x is a vector of dimension n representing motions of p degrees of freedom and u a control vector of dimension p. Suffix m is used to describe the corresponding model states and parameters. Theoretically, the control input that will force the plant to follow the model is given by[3]

$$u = B^{+}(\dot{x}_m - Ax_m) \tag{2}$$

Expanding the system to include actuator dynamics results in

$$\dot{x} = Ax + By \tag{3a}$$

$$\dot{y} = Vy + Ru \tag{3b}$$

where $[V]$ and $[R]$ describe the first-order actuator dynamics. Furthermore, let

$$u = u_F + u_D + u_R \tag{4a}$$

$$e = x - x_m \tag{4b}$$

$$\eta = y - \bar{y} \tag{4c}$$

where e and η are the error vectors resulting from the inaccuracies in the modeling and from external disturbances in actual flight, and

$$u_F = R^{-1}(\dot{\bar{y}} - V\bar{y}) \tag{5}$$

Substituting Eqs. (2), (4), and (5) into Eqs. (3) and simplifying yields

$$\dot{e} = Ae + B\eta \tag{6a}$$

$$\dot{\eta} = V\eta + R(u_R + u_D) \tag{6b}$$

From Eqs. (6), it is evident that the model-following error e has the same dynamics as the basic plant. Hence, to improve the error dynamics and minimize the effect of external disturbances/changes in plant parameters, a proportional-plus-integral feedback must be included.

This inclusion results in

$$\dot{e} = Ae + B\eta \tag{7a}$$

$$\dot{\eta} = RK_1e + V\eta + RK_2w + Ru_D \tag{7b}$$

$$\dot{w} = De \tag{7c}$$

The complete model-following control system including feedback is shown as a block schematic in Fig. 2. The success of this scheme depends on the effective realization of $\dot{\bar{y}}$ and is obtained by using additional filters in cascade. A compromise between the performance and filter complexity led to the choice of the following third-order digital filter:

$$\dot{\bar{y}} = \frac{1}{T_s}\left\{\frac{11}{6}\bar{y}(0) - 3\bar{y}(-1) + \frac{3}{2}\bar{y}(-2) - \frac{1}{3}\bar{y}(-3)\right\} \tag{8}$$

The analysis assumes the number of independent controls to be equal to the degrees of freedom; however, if the number of inputs are less than the number of degrees of freedom, the plant can be partitioned to obtain model following in a reduced number of states. As shown in Ref. 7, this can be achieved by using additional feedback from the plant states that are not to follow the model.

Feedback Control

The feedback gains of the model-following system are selected to minimize the sensitivity of the controlled system to variations in plant parameters and external disturbances. These gains are obtained by using a computer-aided-design technique based on Kreisselmeier and Steinhauser's vector performance optimization.[8] In order to apply the preceding technique, each design objective is formulated quantitatively in terms of a performance criterion. The criterion is selected such that its minimization results in improved performance. The final design compromise is obtained by systematically minimizing the following cost function in several steps:

$$V(k) = \min_k \left\{ \frac{1}{\rho} \ell n \sum_{i=1}^{L} \left[\exp\left(\frac{J_i(k)}{c_i} \right) \right]^{\rho} \right\} \tag{9}$$

where $\rho = 20$ and c_i, the elements of the weighting vector, is selected such that $J_i/c_i \leq 1$. The weights c_i are selected to make J_i/c_i approximately 1, 0.7, or 0.5, depending on whether the corresponding PIV elements J_i are to be minimized further, retained at the same value, or can be allowed to increase.

The different performance criteria used for the longitudinal axes design are now discussed.

The first set of four criteria is output time responses of the controlled aircraft excited by a 3-2-1-1 (or 3-2-1-1 + DC) input. The input is a series of four continous steps with alternating signs, lasting for 3, 2, 1, 1 time units. The length of the time unit can be adjusted to center the frequency band of the input around the system natural frequencies. These measures are computed as a summation over a time interval T_0 to T_f by using a discrete-time equivalent of the equations, as follows:

$$J_i = \int_{T_0}^{T_f} \exp(at) |x_i(t)| \, dt, \quad i = 1, \ldots, 4 \tag{10}$$

The choice of $a \geq 0$ and T_f governs how fast the responses decay and the location of the closed-loop poles. Rate/position limits, time delays, and hysteresis of the actuators are included in the computations of the time responses.

The next set of four criteria considers the disturbance rejection behavior. The system is excited by a filtered white noise input (Dryden spectrum) to obtain gust response measures, as follows:

$$J_{4+i} = \sum_{j=i}^{N} \frac{(x_i - \bar{x}_i)^2}{N}, \quad i = 1, \ldots, 4 \tag{11}$$

where $\bar{x}_i$ is the arithmetic mean of N samples of output x_i.

The third set of eight criteria is derived from singular-value decomposition of the appropriate transfer-function matrices. The measures are used primarily to constrain the feedback gains and to minimize the effect of high-frequency sensor noise. Hence, the transfer-function matrices for both sensor noise and output disturbances are considered for optimization. Minimization of output disturbances can be obtained only at the expense of sensor noise; hence, the desired compromise is dependent on the noise characteristics of the individual sensors. To obtain more flexibility during minimization, modified measures called individual singular values (ISV) are computed. The criteria given in Eqs. (12) are derived in the Appendix.

$$J_{8+i} = \max_{\omega_1 \leq \omega \leq \omega_h} \sigma_{di}\{[I - GK(j\omega)]^{-1}\}, \quad i = 1, \ldots, 4 \tag{12a}$$

$$J_{12+i} = \max_{\omega_1 \leq \omega \leq \omega_h} \sigma_{si}\{[I - GK(j\omega)]^{-1} GK(j\omega)\}, \quad i = 1, \ldots, 4 \tag{12b}$$

The σ_{di} and σ_{si} are maximum ISV's for output disturbances and sensor noise, respectively, and are selected over a frequency range of $\omega_1 = 0.2$ to $\omega_h = 30$ rad/s. These measures are found to be more flexible and effective in limiting the feedback gains than direct-gain constraints.

The last criterion used is based on eigenvalue specifications. Minimizing this criterion below a certain level ensures that all of the closed-loop complex eigenvalue pairs have sufficient damping.

Table 1 Performance index vector optimization

	Step 1		Step 4		Step 7		Step 11	
Criterion	J	c	J	c	J	c	J	c
1	—	—	—	—	4.62	4.62	0.11	0.11
2	—	—	0.14	0.14	0.03	0.05	0.02	0.04
3	0.72	0.72	0.09	0.12	0.08	0.10	0.08	0.12
4	0.31	0.31	0.04	0.06	0.04	0.06	0.04	0.06
5	—	—	—	—	0.63	0.63	0.33	0.33
6	—	—	0.46	0.46	0.25	0.25	0.20	0.20
7	1.71	1.71	1.28	1.28	1.00	1.00	0.82	0.82
8	0.83	0.83	0.38	0.45	0.36	0.50	0.31	0.40
9	—	—	—	—	0.01	0.20	0.20	0.30
10	—	—	0.00	0.20	0.00	0.20	0.00	0.20
11	0.00	0.20	0.05	0.20	0.06	0.20	0.08	0.20
12	0.00	0.20	0.18	0.30	0.20	0.30	0.21	0.30
13	—	—	—	—	0.02	0.50	0.68	0.80
14	—	—	0.00	0.50	0.08	0.50	0.09	0.50
15	0.00	0.50	0.09	0.50	0.11	0.50	0.90	0.50
16	0.00	0.50	0.38	0.60	0.45	0.70	0.58	0.70
17	14.70	14.70	1.72	2.00	1.51	1.60	1.24	2.00
18	—	—	—	—	5.68	7.00	4.30	6.00
19	—	—	0.21	0.25	0.12	0.20	0.10	0.20
20	0.93	1.00	0.16	0.20	0.11	0.20	0.12	0.20
21	0.36	0.50	0.11	0.15	0.10	0.15	0.11	0.15
22	18.10	20.00	2.80	4.00	2.70	4.00	3.00	4.00
23	—	—	—	—	4.08	5.50	3.83	5.50
24	—	—	0.18	0.25	0.20	0.30	0.16	0.30
25	1.08	1.50	0.22	0.30	0.16	0.30	0.12	0.30
26	0.23	0.30	0.09	0.15	0.10	0.15	0.10	0.15
27	12.80	14.00	1.90	3.00	2.00	3.00	1.90	3.00

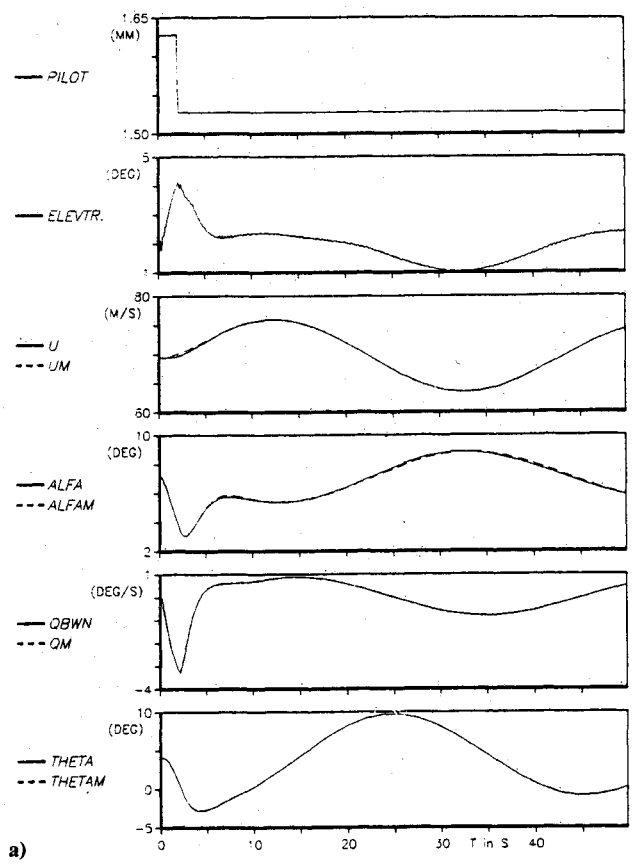

a)

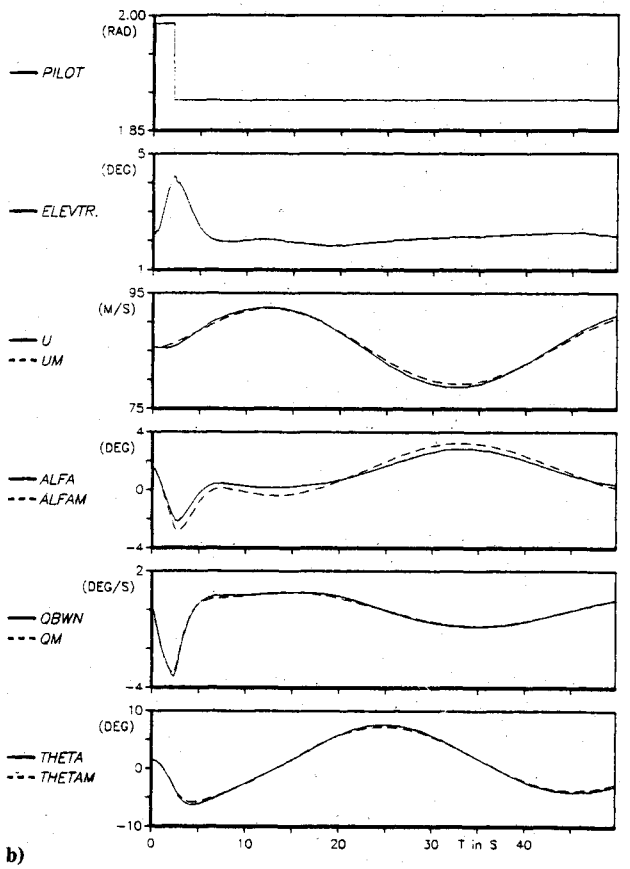

b)

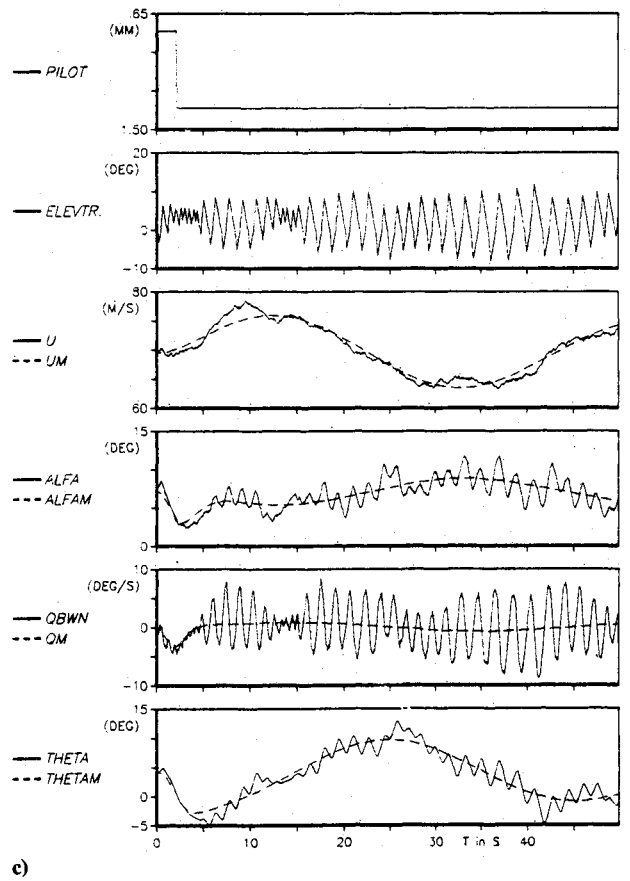

c)

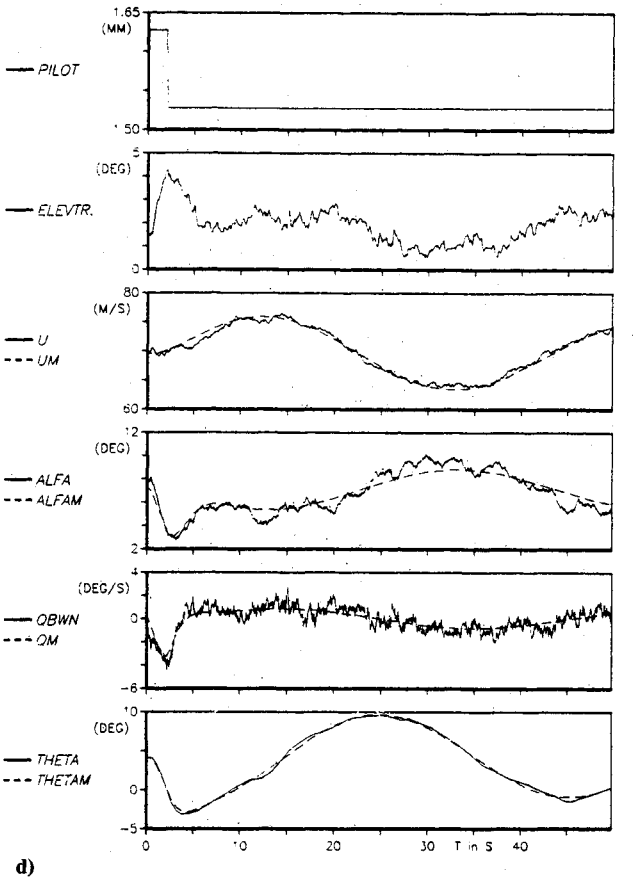

d)

Fig. 3 Nonlinear simulation results: a) controller 2, ideal wind conditions; b) controller 3, ideal wind conditions; c) controller 2, with turbulence; and d) controller 3, with turbulence.

Table 2 Comparison of controller designs

Feedback gains	Design 1	Design 2	Design 3	Individual singular values	Design 1	Design 2	Design 3
$u \to \delta_{th}$, m/s/rad	−0.416	−0.151	−0.060	u_{ext}	6.030	1.146	1.201
$\int u \to \delta_{th}$	−0.031	−0.012	−0.006	u_{sen}	5.945	1.000	0.680
$\alpha \to \delta_f$, rad/rad	1.575	0.242	0.269	α_{ext}	1.258	1.009	1.004
$\int \alpha \to \delta_f$	7.744	1.781	0.393	α_{sen}	0.753	0.128	0.090
$\theta \to \delta_e$, rad/rad	11.155	2.161	1.460	θ_{ext}	1.654	1.211	1.080
$q \to \delta_e$, rad/s/rad	4.465	1.721	0.810	θ_{sen}	0.773	0.134	0.090
$\int \theta \to \delta_e$	2.872	1.007	0.375	q_{ext}	5.786	1.377	1.209
				q_{sen}	5.864	0.868	0.580

$$J_{17} = \max[\mathrm{Im}(\lambda)/\mathrm{Re}(\lambda)] \quad (13)$$

where $\mathrm{Re}(\lambda)$ and $\mathrm{Im}(\lambda)$ are the real and imaginary parts of the complex eigenvalue (λ).

To minimize the sensitivity of the controlled system to variation in the plant parameters caused by changes in flight condition, criteria J_{1-4} and J_{17} are calculated at two additional flight conditions. These conditions are selected to give a maximum variation in dynamic pressure within the "island of operation," for example, low-altitude, high-speed and high-altitude, low-speed flight conditions. Thus, a maximum of 27 (17 + 10) criteria need to be considered for designing the seven feedback gains.

The actual design proceeds in a step-by-step manner, and 10 to 12 individual steps are found to be necessary for obtaining the final design. Table 1 gives the intermediate results and the weighting vectors selected after the third, seventh, and eleventh minimization steps for the design of the longitudinal axes (design 3 in Table 2). This technique guarantees simultaneous reduction of all of the design criteria to the maximum possible percentage relative to the weighting c and, in case of conflicting criteria, enables systematic selection of the best possible compromise (pareto-optimal) solution. The decoupled structure of the feedback gains (q, θ, $\int\theta$, to δ_e, α, $\int\alpha$, to δ_f and u, $\int u$ to δ_{th}—designer's choice), the sequential step-by-step procedure adopted to update the gains and the ability of the designer to interact at each minimization step based on intermediate simulation results, makes the system robust against sensor failures in θ, α, and u. This technique also allows the designer to suitably locate the integral feedback roots; hence, deterioration in overall performance due to saturation in a loop is reduced considerably. Limit detectors (software-controlled) are provided in each individual control loop to detect and isolate the feedback in case the model-following error exceeds a predetermined value for more than a selected duration. Table 2 gives a comparison of three different designs and the corresponding ISV measures. The designs are obtained by using the vector optimization technique, but different sets of PIV elements are used for each design. Design 1 is obtained by using only the time-response measures J_1 to J_4 during minimization. Since no constraints are put on the design results in very high feedback gains, design 2, obtained by using seven additional direct-gain constraints, also restricts the designer's freedom during minimization, thereby increasing the number of iterations needed for the final design. Design 3 includes the complete set of 27 criteria described earlier and is found to yield the most satisfactory result. These examples clearly bring out the need for choosing a proper set of PIV criteria. The success of the method and the design cycle time depend directly on the designer's ability to quantify his or her performance goals effectively and efficiently as elements in the PIV.

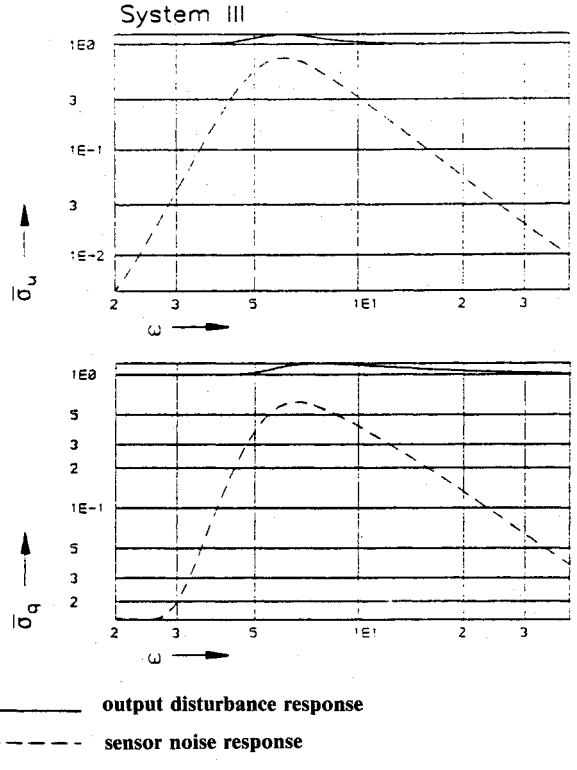

Fig. 4 Two typical individual singular values.

Simulation Results

The results for the landing approach phase of the off-line digital computer simulation are obtained using the nonlinear six-degree-of-freedom simulation package, SIM.[9] Comprehensive actuator models (including hysteresis, time delays, friction, position, and rate limits) and exhaustive engine and airframe data are preprogrammed to make the simulation as exact as possible to the in-flight system.

Figures 3a–3d show one set of typical results obtained for the longitudinal variables, with and without turbulence during model following. A linear model (including first-order actuator dynamics) of a wide-body transport is used for the model. To obtain a common reference, the model variables are transformed to the host aircraft's center of gravity. The responses are obtained by giving a pulse input (of + 5 deg

magnitude and 2 s duration) to the elevator of the model aircraft. This large input results in the control inputs of the host aircraft being operated very close to its performance limits. Controller 2, with higher feedback gains, shows lower model-following errors, but introduction of moderate gusts (Dryden spectrum, $\sigma_w = 1.5$ m/s) results in oscillations as shown in Fig. 3c. Figures 3b and 3d show the performance of controller 3 under identical operating conditions (altitude = 457 m, speed = 68 m/s, $\sigma = 7$ deg). Inspection of the results shows the need to use reasonably high feedback gains to minimize system sensitivity and to reduce model following errors; however, selection of these gains is complicated by the fact that sensor noise, measurement errors, actuator nonlinearities, structural model excitation, etc., limit their magnitude in actual flight.

Conclusions

This paper outlines the technique used for the design of a model-following control system for a new in-flight simulator and includes a set of typical nonlinear simulation results. The inclusion of additional filters in cascade has made the feedforward gains independent of the model even when the actuator dynamics of the host aircraft are modeled explicitly. Existing robustness measures based on singular-value decomposition are modified to yield "new measures" that are included in the performance index vector for optimization. The use of these measures in addition to the time-domain criteria has led to the realization of a more "practical controller" with improved robustness when compared to earlier designs obtained using the same design procedure. The quality of model following using this technique depends on only the exactness of the parameter used to model the host aircraft. To make the host aircraft respond appropriately to turbulence requires a more effective gust-alleviation system, on-line measurement of the gust field, and proper insertion of the measured turbulence into the mode. Currently, efforts are being made in these directions. With the availability of more exact experimental/flight-test data in the near future and with the use of a comprehensive set of performance measures that the technique supports, it is hoped to narrow the gap that exists today between practice and theory.

Appendix

Individual Singular Values

Let

$$\boldsymbol{x}_0 = G(s) \cdot \boldsymbol{u} \tag{A1}$$

where $G(s)$ is the transfer-function matrix between the n vector for output $\boldsymbol{x}_0$ and the p vector for input $\boldsymbol{u}$.

$$G(s) = (sI - A)^{-1}B \tag{A2}$$

The use of spectral norms as measures of matrix size has led to singular-value decomposition being used to characterize performance/stability robustness of multiple-input/multiple-output systems.[10]

By definition

$$\sigma_{\max} \equiv \bar{\sigma} \equiv \sqrt{\lambda^2_{\max}} \tag{A3a}$$

$$\sigma_{\min} \equiv \underline{\sigma} \equiv \sqrt{\lambda^2_{\min}} \tag{A3b}$$

where $\lambda^2_{\max}$ and $\lambda^2_{\min}$ are the maximum and minimum eigenvalues of the positive semi-definite Hermitian matrix

$$G^T(-j\omega) \cdot G(j\omega) \tag{A4}$$

The $\bar{\sigma}$ and $\underline{\sigma}$ are the maximum (minimum) output gains for all possible normalized input combinations, the output and input expressed as Euclidean norms. The related eigenvector gives the amplitude and phase of the input component that generates this maximum (minimum). To obtain effective measures of performance that can be used directly for optimization, the theory is extended to each output variable, i.e., the system is split into n single-output/multi-input systems:

$$\boldsymbol{x}_{0,\nu} = g^T_\nu(s) \cdot \boldsymbol{u} \tag{A5}$$

where $\boldsymbol{x}_{0,\nu}$ is the νth element of the output vector and g^T_ν is the νth row of the transfer-function matrix.

For a given normalized input

$$\boldsymbol{u}^T \cdot \boldsymbol{u} = (\alpha - j\beta)^T \cdot (\alpha + j\beta) = 1 \tag{A6}$$

one can obtain the corresponding output

$$h^2_\nu = (\alpha - j\beta)^T \cdot [g_\nu(-j\omega) \cdot g^T_\nu(j\omega)] \cdot (\alpha + j\beta) \tag{A7}$$

Construct a Lagrangian function $L(\omega)$ with a factor λ^2_ν.

$$L(\omega) = (a - j\beta)^T \cdot [g_\nu(-j\omega) \cdot g^T_\nu(j\omega)] \cdot (\alpha + j\beta) - \lambda^2_\nu[(\alpha - j\beta)^T \cdot (\alpha + j\beta) - 1] \tag{A8}$$

To get the maximum of $L(\omega)$, the gradients of L with respect to α_ν and β_ν must be made equal to zero, i.e.,

$$[g_\nu(-j\omega) \cdot g^T_\nu(j\omega)] \cdot (\alpha + j\beta) - \lambda^2_\nu(\alpha + j\beta) = 0 \tag{A9}$$

The range of $[g(-j\omega) \cdot g^T(j\omega)]$ is 1 and because the matrix is positive definite there exists $\lambda_\nu = \lambda_{\nu\max} > 0$. And, inserting λ_ν from Eq. (A9) into Eq. (A7) using Eq. (A6), yields

$$h_{\nu\max} = \lambda_{\nu\max}(\omega) \tag{A10}$$

where $h_{\nu\max}$ is the maximum output amplitude of the νth variable for all possible normalized input combinations of amplitude and phase for the given frequency ω. One can obtain an individual $\lambda_{\nu\max}$ for all outputs over a frequency range of interest and use these as measures of disturbance suppression in each variable $x_{0,\nu}$. By choosing the appropriate transfer functions depending on where the noise/disturbance enters the system, one can obtain several measures. Figure 4 shows typical ISV plots for pitch rate (q) and forward velocity (u) obtained using controller 3 (Table 2).

References

[1]Hanke, D., "Der fliegende Simulator und Technologieträger ATTAS der DFVLR," Luft- und Raumfahrt, Vol. 7, Jan. 1986, pp. 4–8.

[2]Henschel, F., "On Control Concepts for In-flight Simulation Including Actuator Nonlinearities and Time Delays," European Space Agency TT-948, 1985.

[3]Motyka, P. R., Rynaski, E. G., and Reynolds, P. A., "Theory and Flight Verification of the TIFS Model Following System," *Journal of Aircraft*, Vol. 9, May 1972, pp. 347–353.

[4]Asseo, S. J., "On the Optimal Gain Problem and Its Application," Joint Automatic Control Conference, Univ. of Michigan, Ann Arbor, MI, 1969.

[5]Kawahata, N., "Model Following System with Assignable Error Dynamics and Its Application to Aircraft," *Journal of Guidance and Control*, Vol. 3, Nov.–Dec. 1980, pp. 508–516.

[6]Tsukano, Y., Komoda, M., Kawahata, N., and Ono, T., "Variable Stability and Response Airplane System and Its Flight Verification," *Journal of the Japan Society for Aeronautical and Space Science*, Vol. 31, No. 349, 1983.

[7]Rynaski, E. G., "Adaptive Control Application to Aircraft," *Applications of Adaptive Control*, Academic, New York, 1980, pp. 259–265.

[8]Kreisselmeier, G. and Steinhauser, R., "Systematic Control Design by Optimizing a Vector Performance Index," *IFAC Symposium on Computer Aided Design of Control Systems*, Aug. 1979, pp. 113–117.

[9]Mackie, D., "Handbuch für das System zur Flugsimulation," DFVLR IB 111-83/5, Jan. 1983.

[10]Doyle, J. C. and Stein, G., "Multivariable Feedback Design: Concepts for Classical/Modern Synthesis," *IEEE Transactions on Automatic Control*, Vol. AC-26, No. 1, Feb. 1981, pp. 4–16.